

Screening magnetic two-dimensional atomic crystals with nontrivial electronic topology

Hang Liu,^{†,¶} Jia-Tao Sun,^{*,†,¶} Miao Liu,[†] and Sheng Meng^{*,†,‡,¶}

[†] Beijing National Laboratory for Condensed Matter Physics and Institute of Physics, Chinese Academy of Sciences, Beijing 100190, People's Republic of China

[‡] Collaborative Innovation Center of Quantum Matter, Beijing 100190, People's Republic of China

[¶] University of Chinese Academy of Sciences, Beijing 100049, People's Republic of China

Corresponding Authors

*E-mail: jtsun@iphy.ac.cn (J.T.S.).

*E-mail: smeng@iphy.ac.cn (S.M.).

ABSTRACT: To date only a few two-dimensional (2D) magnetic crystals were experimentally confirmed, such as CrI₃ and CrGeTe₃, all with very low Curie temperatures (T_C). High-throughput first-principles screening over a large set of materials yields 89 magnetic monolayers including 56 ferromagnetic (FM) and 33 antiferromagnetic compounds. Among them, 24 FM monolayers are promising candidates possessing T_C higher than that of CrI₃. High T_C monolayers with fascinating electronic phases are identified: (i) quantum anomalous and valley Hall effects coexist in a single material RuCl₃ or VC₃, leading to a valley-polarized quantum anomalous Hall state; (ii) TiBr₃, Co₂NiO₆ and V₂H₃O₅ are revealed to be half-metals. More importantly, a new type of fermion dubbed type-II Weyl ring is discovered in ScCl. Our work provides a database of 2D magnetic materials, which could guide experimental realization of high-temperature magnetic monolayers with exotic electronic states for future spintronics and quantum computing applications.

KEYWORDS: Magnetic two-dimensional crystals, high throughput calculations, quantum anomalous Hall effect, valley Hall effect.

The discovery of two-dimensional (2D) materials opens a new avenue with rich physics promising for applications in a variety of subjects including optoelectronics, valleytronics, and spintronics, many of which benefit from the emergence of Dirac/Weyl fermions. One example is transition-metal dichalcogenide (TMDC) monolayers, whose finite direct bandgap enable novel optoelectronic controls as well as valley-dependent phenomena, such as circular dichroism and valley Hall effect (VHE)¹⁻². Due to the equivalent occupation of K and K' valleys in TMDC materials, the VHE does not produce observable macroscopic Hall voltage. This is overcome in magnetic counterparts, resulted from time reversal symmetry breaking³⁻⁸. In contrast to fermions in nonmagnetic systems, such as massless Dirac fermions in borophene, black phosphorus, Cu_2Si ⁹⁻¹³, and massive Dirac fermions in graphene and bilayer bismuth¹⁴⁻¹⁵, few types of fermions in 2D magnetic systems are proposed, implying the scarcity of intrinsic magnetic 2D crystals. In particular, 2D magnets with massive Dirac fermions can support quantum anomalous Hall state leading to topologically protected spin current, promising for low-power-consumption devices. Unfortunately, the state is only realized in 2D materials with non-intrinsic magnetism at extremely low temperature (e.g. 30 mK for Cr-doped $(\text{Bi,Sb})_2\text{Te}_3$ thin film)¹⁶⁻²², hampering its extensive applications. Therefore, discovery of 2D magnets at an elevated temperature is of great importance, providing optimal platforms to enable realistic spintronic and quantum devices, as well as to realize new electronic states.

To date 2D magnetic materials are limited to marginal modifications to existing compounds, for instance by: (i) adsorbing hydrogen on graphene²³; (ii) reconstructing surface/edge²⁴⁻²⁵; or (iii) creating defects in MoS_2 nanosheets²⁶. The intrinsic 2D ferromagnetism has only been observed in atomically thin CrI_3 and CrGeTe_3 , only accessible at a low temperature of ~ 40 K²⁷⁻²⁸. The absence of ideal 2D magnetic materials indicates that traditional trial-and-error approaches to discover new materials are not effective. Recently, computational screening from existing material databases presents an essential tool to accelerate materials discovery²⁹⁻³⁸. Hence, the big challenge to identify monolayer magnets may be addressed by high-throughput calculations based on density functional theory.

In this work, we employ high-throughput first-principles calculations to systematically screen monolayer materials with intrinsic magnetism at a high temperature, better if they are equipped with nontrivial topological properties. We have successfully identified 56 ferromagnetic (FM) monolayers, including 24 monolayers with a Curie temperature (T_C) higher than that of monolayer CrI_3 . We also find that quantum anomalous and valley Hall effect coexist in FM monolayers of VCI_3 and RuCl_3 , supporting the native existence of valley-polarized, topologically protected, quantized spin current. Monolayer ScCl possesses 2D type-II Weyl nodal ring centering on Γ point, which may lead to intriguing electronic properties beyond known fermions. Our work provides a rich data set of materials potentially supporting high-temperature 2D magnetism as well as new topological states.

The computational screening process is schematically shown in Figure 1. We start from a 2D materials database obtained by screening Materials Project data (with $\sim 65,000$ entries) using the topology-scaling algorithm²⁹. As shown in Figure 2(a), 627 monolayer materials including 7 unary, 220 binary, 323 ternary, 69 quaternary and 8 quinary 2D compounds, have the exfoliation energy below that of experimentally existing SnSe monolayer (150 meV/atom)²⁹. To investigate their magnetic properties, spin polarized calculations with collinear

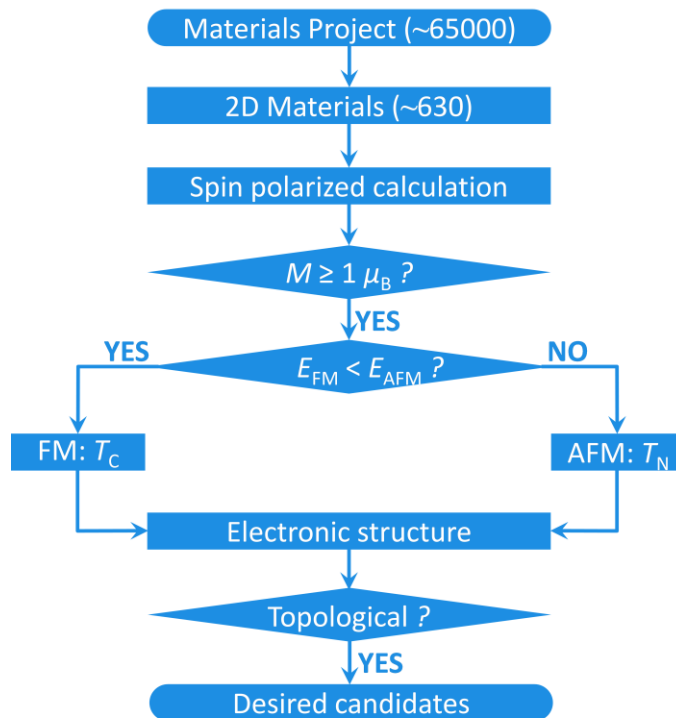


Figure 1. Flow chart of computational high-throughput screening.

magnetic configurations are carried out, where the initial magnetic moment is set as $6 \mu_B$ for each magnetic atom. Only materials with the final magnetic moment larger than $1 \mu_B/\text{unit cell}$ are selected as 2D magnetic candidates for further computation. This screening process yields 89 magnetic monolayers, including 33 binary, 39 ternary, 13 quaternary and 4 quinary compounds. As shown in Figure 2b. It is clear that ternary compounds top the list, followed by binary, quaternary, and quinary compounds. All magnetic monolayers contain transition metal (TM) atoms, indicating that the design of magnetic monolayers should be restricted to TM-containing materials.

To determine magnetic ground state, the total energy of antiferromagnetic (AFM) state (E_{AFM}) is compared with that of FM state (E_{FM}). With regard to the magnetic structure of AFM state, checkerboard configuration is adopted preferentially. When the self-consistence convergence of computation fails for checkerboard case, stripe configuration is also considered (see Figure S1 for details about magnetic configurations³⁹). As shown in Figure 2c, 2d, 2e, there are 56 (33) FM (AFM) monolayers, consisting of 21 (12) binary, 27 (12) ternary, 6 (7) quaternary and 2 (2) quinary compounds. Binary FM monolayers are mostly halides, while chalcogenides dominate ternary magnetic monolayers. The magnetic monolayers can be further classified by their structural prototypes. Binary magnetic compounds mainly include the prototypes with composition of XY_2 and XY_3 , possessing space groups of $P\bar{3}m1$ and $P\bar{3}1m$, respectively. Anions therein belong to VI A and VII A groups of elements, and cations are mostly from the TMs in the fourth and fifth element rows. Unlike the binaries, there are rich structural prototypes for ternary compounds, which can be used as prototypes to extend the candidate list to a larger compositional space by atomic substitution. This candidate list also serves as a guidance towards experimental synthesis of FM and AFM monolayers (see Table S1, S2 and S3 for details³⁹).

Next, the Curie (Néel) temperature T_C (T_N) is calculated to give the upper limit of the transition temperature of screened FM (AFM) monolayers. The critical transition temperature of ferromagnets T_C and antiferromagnets T_N in the mean field approximation is calculated by

40-43

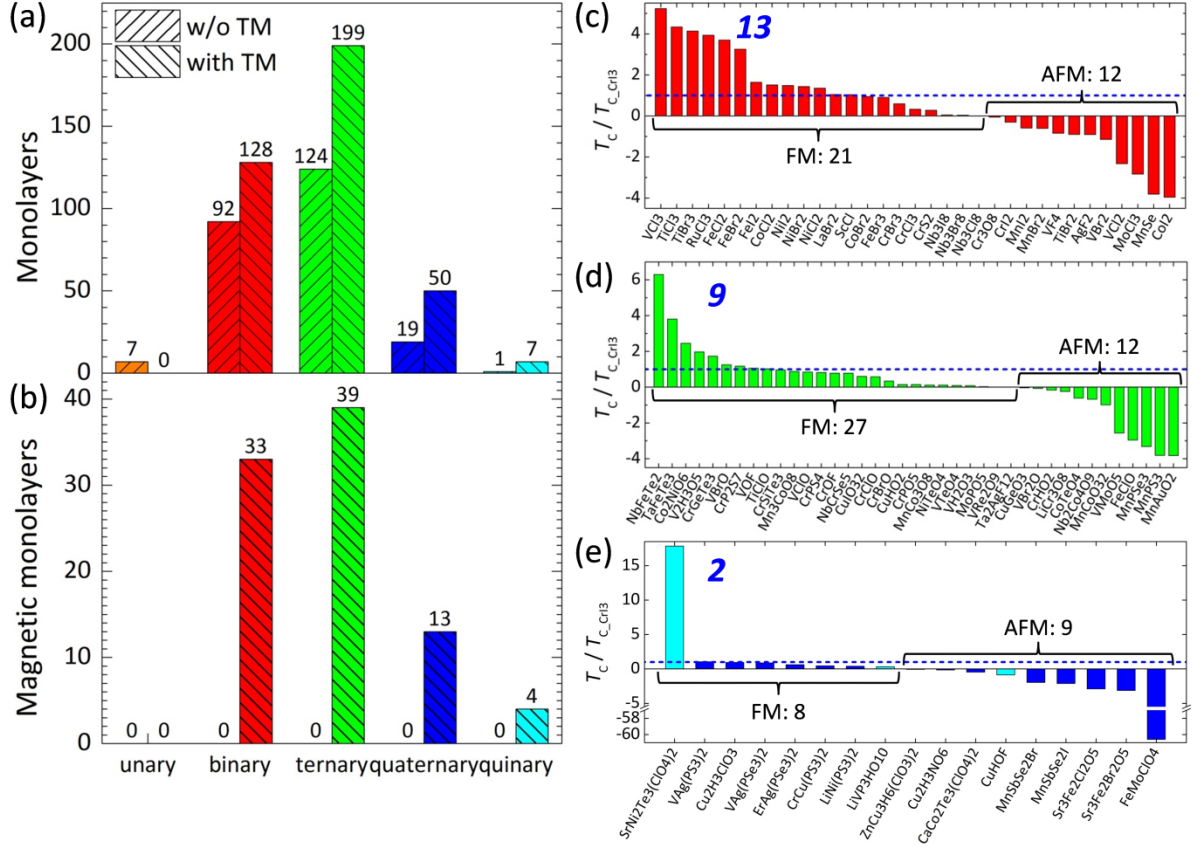


Figure 2. Screened magnetic monolayer materials. (a) The initial 627 monolayer materials are classified as unary (orange), binary (red), ternary (green), quaternary (blue) and quinary (cyan). Every classification is classified further according to whether it contains TM atom or not. (b) Classification of 89 magnetic monolayers with magnetic moment larger than $1 \mu_B$ /unit cell. Curie temperature of magnetic binary (c), ternary (d), quaternary and quinary (e) monolayers.

$$E_{AFM} - E_{FM} = N \frac{3}{2} k_B T_{C(N)}, \quad (1)$$

where E_{FM} and E_{AFM} are the total energy of magnetic monolayers with N magnetic atoms in ferromagnetic and antiferromagnetic states, respectively. Here k_B denotes the Boltzmann constant. The critical transition temperature of the 89 magnetic monolayers is shown in Figures. 2c, 2d, 2e, as grouped by the number of atomic species. The T_C of CrX_3 ($CrXTe_3$) monolayers decrease as element X is replaced by I, Br, Cl (Ge, Si) successively, which is consistent with Monte Carlo simulations⁴⁴⁻⁴⁵. This indicates that, although the absolute value of $T_{C(N)}$ in Eq. (1) is a rough estimation, the qualitative comparison between different materials is reasonable. In the same spirit, the calculated $T_{C(N)}$ from mean field approximation

is corrected by rescaling $\frac{T_{C(N)_cor}}{T_{C(N)}} = \frac{T_{C_exp}|_{CrI_3}}{T_C|_{CrI_3}}$, where $T_{C(N)_cor}$ is the corrected value, and $T_{C_exp}|_{CrI_3} = 45$ K is experimental T_C of CrI_3 ²⁷.

Similar to previous reports on engineering T_C by atomic substitution in CrX_3 and $CrXTe_3$ monolayers⁴⁴⁻⁴⁵, new materials supporting the same behaviors have been identified. By replacing chemical element from Cl, Br to I successively, T_C in FM monolayers of NiX_2 , VX_2 and MnX_2 increases gradually. In contrast, this behavior in systems of FeX_2 and CoX_2 is reversed. Specially, the T_C of CoX_2 decreases so significantly that it becomes a negative value for CoI_2 , manifesting the change from FM state in $CoCl_2$ and $CoBr_2$ to AFM state in CoI_2 . Along with this transition of magnetic order, electronic structure changes from semiconducting in $CoCl_2$ and $CoBr_2$ to metallic in CoI_2 . Hence, phase transitions between FM (semiconducting) and AFM (metallic) states can be realized by doping iodine atoms in $CoCl_2$ or $CoBr_2$, offering an alternative way to engineer magnetism⁴⁶⁻⁴⁷.

The Curie temperature of FM CrI_3 monolayer ($T_C|_{CrI_3} = 290$ K) is taken as a reference to screen high-temperature 2D magnets. As shown in Figures 2c, 2d, 2e, we identified 24 FM monolayers, including 13 binary, 9 ternary, 1 quaternary and 1 quinary compounds, to have T_C higher than that of CrI_3 . This implies that FM order in these materials can be observed at higher temperature than that of CrI_3 . Among them, new semiconductors ($CoCl_2$, NiI_2 , $NiBr_2$, $NiCl_2$, $LaBr_2$, $CrGeTe_3$, and CrP_2S_7), new semimetals (VCl_3 , $RuCl_3$, and $ScCl$), new half-metals ($TiBr_3$, Co_2NiO_6 , and $V_2H_3O_5$), and new metals ($NbFeTe_2$ and $TaFeTe_3$) are proposed (see Figures. S2, S3, S4 for details³⁹). Besides binary and ternary compounds, monolayers with more types of chemical elements are also promising candidates for 2D spintronic applications. For example, the T_N of $FeMoClO_4$ is 60 times higher than $T_C|_{CrI_3}$, suggesting a great potential to be used in realistic devices.

Because of time reversal symmetry breaking, magnetic monolayers identified above may host topologically nontrivial physics. Monolayer $RuCl_3$ exhibits $T_C = 4.0 \times T_C|_{CrI_3}$, and each Ru atom possesses in-plane magnetic moment of $1 \mu_B$ (Figure 3a). When spin-orbit coupling (SOC) is not considered, there are six spin polarized massless Dirac cones along ΓM path, shown in Figure 3b. When SOC is considered, all the massless Dirac cones become massive,

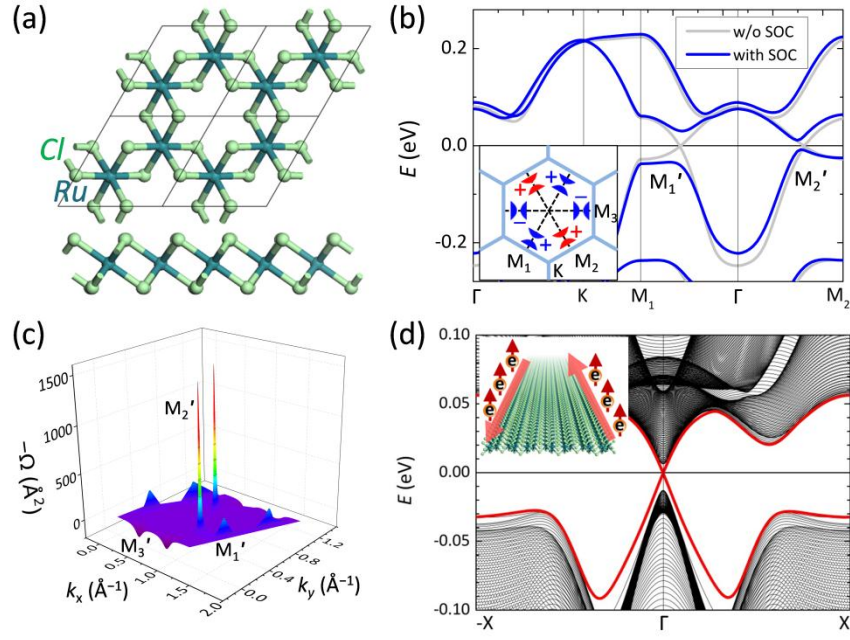


Figure 3. Quantum anomalous Hall state in ferromagnetic monolayer RuCl₃. (a) Atomic structure of RuCl₃. (b) Band structure of RuCl₃ with (blue line) and without SOC (gray line). The inset shows all the massive Dirac cones and corresponding sign of Berry curvature. (c) Berry curvature in FBZ. (d) Band structure of RuCl₃ nanoribbon with a width of 386 Å. The red line shows the topologically protected edge states. The inset shows quantized spin current on two edges.

leading to four valleys with band gap of 64 meV (M_1' , M_3') and two valleys with band gap of 19 meV (M_2'). To further characterize the insulating state, we calculate the Chern number

$C = \frac{1}{2\pi} \sum_n \int_{BZ} d^2k \Omega_n$. The momentum-space Berry curvature Ω_n for the n th band is given by^{22,48}

$$\Omega_n(k) = -\sum_{n' \neq n} \frac{2 \text{Im} \langle \psi_{nk} | \hat{v}_x | \psi_{n'k} \rangle \langle \psi_{n'k} | \hat{v}_y | \psi_{nk} \rangle}{(E_{n'} - E_n)^2}, \quad (2)$$

where n and n' are band indexes, \hat{v}_x and \hat{v}_y are velocity operators along x and y directions. As shown in Figures 3b and 3c, the sign of Berry curvature around M_3' valley is opposite to that of M_1' and M_2' valleys, leading to opposite anomalous velocity of electrons from M_3' and M_1' , M_2' valleys under the in-plane electric field. This phenomenon is known as VHE⁴⁹. Specially, natively measurable valley Hall voltage appears, resulted from inequivalent numbers of valley electrons with positive and negative Berry curvature.

Integrating the Berry curvature in the first Brillouin zone (FBZ) leads to nonzero Chern number $C = -1$, indicating that FM monolayer RuCl₃ exhibits QAHE. The calculated Chern

number is consistent with the band structure of RuCl_3 nanoribbon with a width of 386 \AA , where there is one quantized spin polarized current channel protected from scattering on each edge (Figure 3d). Compared with previous works to realize QAHE by magnetic doping¹⁷ or functionalizing 2D materials^{20,50}, the valley-polarized QAHE (v-QAHE) emerges in intrinsic magnetic RuCl_3 at high temperature, much easier to be realized in experiments and utilized in devices. Besides, the coexistence of intrinsic QAHE and natively polarized VHE in monolayer RuCl_3 indicates that it is a good platform to study the interplay between QAHE and VHE. Similarly, monolayer VC_3 with $C = 1$ also supports the v-QAHE (see details in Figure S5³⁹). However, in contrast with completely in-plane magnetic moment of RuCl_3 , the magnetic moment of VC_3 has out-of-plane component, which is promising for hosting intriguing non-collinear and non-coplanar spin chirality⁵¹.

Besides the superior materials to realize already-known states, new electronic state is also identified. The FM monolayer ScCl_3 , with magnetic moment of $1.5 \mu_B/\text{unit cell}$ and $T_C = 1.03 \times T_{C|\text{CrI}_3}$, consists of two chlorine atomic layers intercalated by two scandium atomic layers (see Figure 4a). As shown in Figures 4b and 4c, spin-up and spin-down bands cross with each

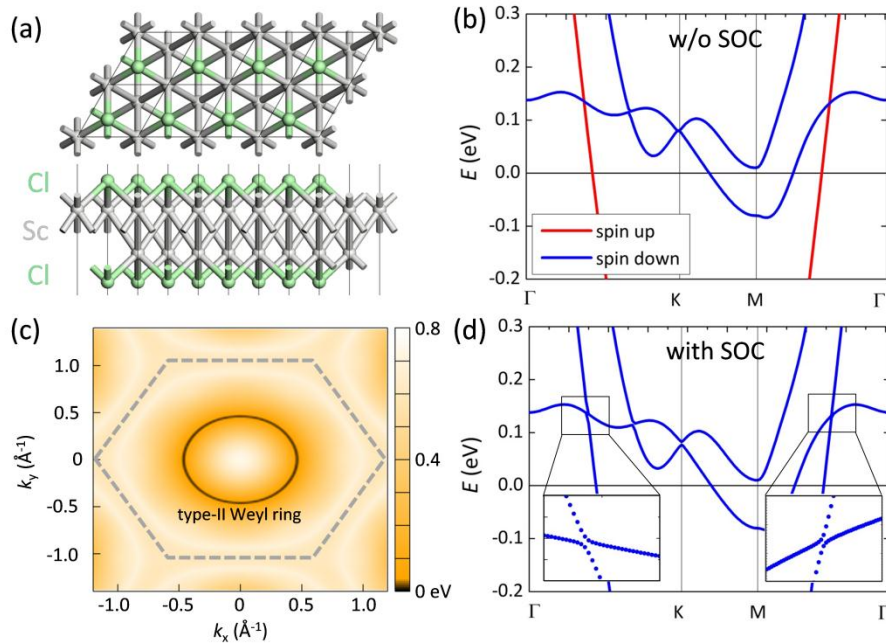


Figure 4. 2D Type-II Weyl ring in ferromagnetic monolayer ScCl_3 . (a) Atomic structure of monolayer ScCl_3 . (b) Bandstructure without SOC. Bandstructure with SOC (d) and location of type-II Weyl ring (c).

other at the energy of 0.13 eV, resulting in a nodal ring around Γ point. Each crossing point on this ring is double degenerate, which is different from quadruple Dirac ring in 2D Cu_2Si ¹¹. Moreover, because each cone on the ring has type-II band dispersion, it is dubbed type-II Weyl ring here, which may possess intriguing topologically nontrivial electronic properties. Due to weak SOC of Sc and Cl atoms, the band gap on the ring is negligible, as shown in Figure 4d. This type-II Weyl ring almost occupies half of the FBZ [Figure 4c], leading to easy observation in experiment using e.g. angle resolved photoemission spectroscopy.

In conclusion, we have identified 89 magnetic monolayers, including 33 binary, 39 ternary, 13 quaternary and 4 quinary compounds through high-throughput computational screening based on first-principles calculations. We find 24 monolayers with higher T_C than that of experimentally confirmed ferromagnet CrI_3 . Furthermore, from these high T_C monolayers, new half-metals TiBr_3 , Co_2NiO_6 and $\text{V}_2\text{H}_3\text{O}_5$ are proposed, and new ferromagnets RuCl_3 and VC_3 are found to support valley-polarized QAHE. Besides, novel electronic state named type-II Weyl ring is predicted in monolayer ferromagnetic ScCl . Our work provides a significant clue to realize 2D high-temperature ferromagnets with novel Dirac/Weyl fermions. This work may stimulate further investigations on the effect of layer thickness, magnetic configurations, light-magnetism interaction of these magnetic 2D crystals.

■ ASSOCIATED CONTENT

* Supporting Information

The Supporting Information is available free of charge on the ACS Publications website at DOI: XXX.XXX.

It includes the following parts: computational methods, magnetic configurations, the atomic and electronic structures of semiconducting, metallic, half-metallic 2D magnetic materials with high T_C .

■ AUTHOR INFORMATION

Corresponding Authors

*E-mail: jtsun@iphy.ac.cn (J.T.S.).

*E-mail: smeng@iphy.ac.cn (S.M.).

Notes

The authors declare no competing financial interest.

■ ACKNOWLEDGEMENTS

This work was financially supported by the National Key Research and Development Program of China (Grants No. 2016YFA0202300, No. 2016YFA0300902, No. 2015CB921001), National Basic Research Program of China (Grants No. 2013CBA01600), National Natural Science Foundation of China (Grants No. 11774396 and

No. 61306114), "Strategic Priority Research Program (B)" of Chinese Academy of Sciences (Grants No. XDB30000000 and No. XDB07030100).

■ REFERENCES

1. Lopez-Sanchez, O.; Lembke, D.; Kayci, M.; Radenovic, A.; Kis, A. Ultrasensitive photodetectors based on monolayer MoS₂. *Nat. Nanotechnol.* **2013**, *8*, 497-501.
2. Batmunkh, M.; Bat-Erdene, M.; Shapter, J. G. Phosphorene and Phosphorene-Based Materials - Prospects for Future Applications. *Adv. Mater.* **2016**, *28*, 8586-8617.
3. Liu, J.; Hou, W.-J.; Cheng, C.; Fu, H.-X.; Sun, J.-T.; Meng, S. Intrinsic valley polarization of magnetic VSe₂ monolayers. *Journal of Physics: Condensed Matter* **2017**, *29*, 255501.
4. Sun, J.-T.; Wang, Z.; Meng, S.; Du, S.; Liu, F.; Gao, H. J. Spin-polarized valley Hall effect in ultrathin silicon nanomembrane via interlayer antiferromagnetic coupling. *2D Materials* **2016**, *3*, 035026.
5. Smoleński, T.; Goryca, M.; Koperski, M.; Faugeras, C.; Kazimierzuk, T.; Bogucki, A.; Nogajewski, K.; Kossacki, P.; Potemski, M. Tuning Valley Polarization in a WSe₂ Monolayer with a Tiny Magnetic Field. *Phys. Rev. X* **2016**, *6*, 021024.
6. Marino, E. C.; Nascimento, L. O.; Alves, V. S.; Smith, C. M. Interaction Induced Quantum Valley Hall Effect in Graphene. *Phys. Rev. X* **2015**, *5*, 011040.
7. Wang, Z.; Mak, K. F.; Shan, J. Strongly Interaction-Enhanced Valley Magnetic Response in Monolayer WSe₂. *Phys. Rev. Lett.* **2018**, *120*, 066402.
8. Li, Y.; Ludwig, J.; Low, T.; Chernikov, A.; Cui, X.; Arefe, G.; Kim, Y. D.; van der Zande, A. M.; Rigosi, A.; Hill, H. M.; Kim, S. H.; Hone, J.; Li, Z.; Smirnov, D.; Heinz, T. F. Valley splitting and polarization by the Zeeman effect in monolayer MoSe₂. *Phys. Rev. Lett.* **2014**, *113*, 266804.
9. Feng, B.; Sugino, O.; Liu, R. Y.; Zhang, J.; Yukawa, R.; Kawamura, M.; Iimori, T.; Kim, H.; Hasegawa, Y.; Li, H.; Chen, L.; Wu, K.; Kumigashira, H.; Komori, F.; Chiang, T. C.; Meng, S.; Matsuda, I. Dirac Fermions in Borophene. *Phys. Rev. Lett.* **2017**, *118*, 096401.
10. Kim, J.; Baik, S. S.; Jung, S. W.; Sohn, Y.; Ryu, S. H.; Choi, H. J.; Yang, B.-J.; Kim, K. S. Two-Dimensional Dirac Fermions Protected by Space-Time Inversion Symmetry in Black Phosphorus. *Phys. Rev. Lett.* **2017**, *119*, 226801.
11. Feng, B.; Fu, B.; Kasamatsu, S.; Ito, S.; Cheng, P.; Liu, C.-C.; Feng, Y.; Wu, S.; Mahatha, S. K.; Sheverdyeva, P.; Moras, P.; Arita, M.; Sugino, O.; Chiang, T.-C.; Shimada, K.; Miyamoto, K.; Okuda, T.; Wu, K.; Chen, L.; Yao, Y.; Matsuda, I. Experimental realization of two-dimensional Dirac nodal line fermions in monolayer Cu₂Si. *Nat. Commun.* **2017**, *8*, 1007.
12. Gao, L.; Sun, J. T.; Lu, J. C.; Li, H.; Qian, K.; Zhang, S.; Zhang, Y. Y.; Qian, T.; Ding, H.; Lin, X.; Du, S.; Gao, H. J. Epitaxial Growth of Honeycomb Monolayer CuSe with Dirac Nodal Line Fermions. *Adv. Mater.* **2018**, *30*, 1707055.
13. Liu, H.; Sun, J.-T.; Cheng, C.; Liu, F.; Meng, S. Photoinduced Nonequilibrium Topological States in Strained Black Phosphorus. *Phys. Rev. Lett.* **2018**, *120*, 237403.
14. Drozdov, I. K.; Alexandradinata, A.; Jeon, S.; Nadj-Perge, S.; Ji, H.; Cava, R. J.; Andrei Bernevig, B.; Yazdani, A. One-dimensional topological edge states of bismuth bilayers. *Nat. Phys.* **2014**, *10*, 664-669.
15. Kane, C. L.; Mele, E. J. Quantum spin Hall effect in graphene. *Phys. Rev. Lett.* **2005**, *95*, 226801.
16. Yu, R.; Zhang, W.; Zhang, H.-J.; Zhang, S.-C.; Dai, X.; Fang, Z. Quantized Anomalous Hall Effect in Magnetic Topological Insulators. *Science* **2010**, *329*, 61-64.
17. Chang, C.-Z.; Zhang, J.; Feng, X.; Shen, J.; Zhang, Z.; Guo, M.; Li, K.; Ou, Y.; Wei, P.; Wang, L.-L.; Ji, Z.-Q.; Feng, Y.; Ji, S.; Chen, X.; Jia, J.; Dai, X.; Fang, Z.; Zhang, S.-C.; He, K.; Wang, Y.; Lu, L.; Ma, X.-C.; Xue, Q.-K. Experimental Observation of the Quantum Anomalous Hall Effect in a Magnetic Topological Insulator.

Science **2013**, *340*, 167-170.

18. Liu, C. X.; Qi, X. L.; Dai, X.; Fang, Z.; Zhang, S. C. Quantum anomalous hall effect in $\text{Hg}_{(1-y)}\text{Mn}_y\text{Te}$ quantum wells. *Phys. Rev. Lett.* **2008**, *101*, 146802.
19. Hsu, C.-H.; Fang, Y.; Wu, S.; Huang, Z.-Q.; Crisostomo, C. P.; Gu, Y.-M.; Zhu, Z.-Z.; Lin, H.; Bansil, A.; Chuang, F.-C.; Huang, L. Quantum anomalous Hall insulator phase in asymmetrically functionalized germanene. *Phys. Rev. B* **2017**, *96*, 165426.
20. Liang, Q.-F.; Zhou, J.; Yu, R.; Wang, X.; Weng, H. Interaction-driven quantum anomalous Hall effect in halogenated hematite nanosheets. *Phys. Rev. B* **2017**, *96*, 205412.
21. Fu, H.; Ren, J.; Chen, L.; Si, C.; Qiu, J.; Li, W.; Zhang, J.; Sun, J.; Li, H.; Wu, K.; Duan, W.; Meng, S. Prediction of silicon-based room temperature quantum spin Hall insulator via orbital mixing. *EPL (Europhysics Letters)* **2016**, *113*, 67003.
22. Fu, H.; Liu, Z.; Lian, C.; Zhang, J.; Li, H.; Sun, J.-T.; Meng, S. Magnetic Dirac fermions and Chern insulator supported on pristine silicon surface. *Phys. Rev. B* **2016**, *94*, 035427.
23. Gonzalez-Herrero, H.; Gomez-Rodriguez, J. M.; Mallet, P.; Moaied, M.; Jose Palacios, J.; Salgado, C.; Ugeda, M. M.; Veullen, J.-Y.; Yndurain, F.; Brihuega, I. Atomic-scale control of graphene magnetism by using hydrogen atoms. *Science* **2016**, *352*, 437-441.
24. Son, Y. W.; Cohen, M. L.; Louie, S. G. Half-metallic graphene nanoribbons. *Nature* **2006**, *444*, 347-9.
25. Liu, H.; Sun, J.-T.; Fu, H.-X.; Sun, P.-J.; Feng, Y. P.; Meng, S. All-Silicon Switchable Magnetoelectric Effect through Interlayer Exchange Coupling. *ChemPhysChem* **2017**, *18*, 1916-1920.
26. Cai, L.; He, J.; Liu, Q.; Yao, T.; Chen, L.; Yan, W.; Hu, F.; Jiang, Y.; Zhao, Y.; Hu, T.; Sun, Z.; Wei, S. Vacancy-induced ferromagnetism of MoS_2 nanosheets. *J. Am. Chem. Soc.* **2015**, *137*, 2622-7.
27. Huang, B.; Clark, G.; Navarro-Moratalla, E.; Klein, D. R.; Cheng, R.; Seyler, K. L.; Zhong, D.; Schmidgall, E.; McGuire, M. A.; Cobden, D. H.; Yao, W.; Xiao, D.; Jarillo-Herrero, P.; Xu, X. Layer-dependent ferromagnetism in a van der Waals crystal down to the monolayer limit. *Nature* **2017**, *546*, 270-273.
28. Gong, C.; Li, L.; Li, Z.; Ji, H.; Stern, A.; Xia, Y.; Cao, T.; Bao, W.; Wang, C.; Wang, Y.; Qiu, Z. Q.; Cava, R. J.; Louie, S. G.; Xia, J.; Zhang, X. Discovery of intrinsic ferromagnetism in two-dimensional van der Waals crystals. *Nature* **2017**, *546*, 265.
29. Ashton, M.; Paul, J.; Sinnott, S. B.; Hennig, R. G. Topology-Scaling Identification of Layered Solids and Stable Exfoliated 2D Materials. *Phys. Rev. Lett.* **2017**, *118*, 106101.
30. Mounet, N.; Gibertini, M.; Schwaller, P.; Campi, D.; Merkys, A.; Marrazzo, A.; Sohler, T.; Castelli, I. E.; Cepellotti, A.; Pizzi, G.; Marzari, N. Two-dimensional materials from high-throughput computational exfoliation of experimentally known compounds. *Nat. Nanotechnol.* **2018**, *13*, 246.
31. Bjorkman, T.; Gulans, A.; Krashennikov, A. V.; Nieminen, R. M. Van der Waals bonding in layered compounds from advanced density-functional first-principles calculations. *Phys. Rev. Lett.* **2012**, *108*, 235502.
32. Lebègue, S.; Bjorkman, T.; Klintonberg, M.; Nieminen, R. M.; Eriksson, O. Two-Dimensional Materials from Data Filtering and Ab Initio Calculations. *Phys. Rev. X* **2013**, *3*, 031002.
33. Rhone, T. D.; Chen, W.; Desai, S.; Yacoby, A.; Kaxiras, E. Data-driven studies of magnetic two-dimensional materials. *arXiv:1806.07989*.
34. Ataca, C.; Şahin, H.; Ciraci, S. Stable, Single-Layer MX_2 Transition-Metal Oxides and Dichalcogenides in a Honeycomb-Like Structure. *The Journal of Physical Chemistry C* **2012**, *116*, 8983-8999.
35. Rasmussen, F. A.; Thygesen, K. S. Computational 2D Materials Database: Electronic Structure of Transition-Metal Dichalcogenides and Oxides. *The Journal of Physical Chemistry C* **2015**, *119*, 13169-13183.
36. Hachmann, J.; Olivares-Amaya, R.; Atahan-Evrenk, S.; Amador-Bedolla, C.; Sánchez-Carrera, R. S.; Gold-Parker, A.; Vögt, L.; Brockway, A. M.; Aspuru-Guzik, A. n. The Harvard Clean Energy Project: Large-Scale

- Computational Screening and Design of Organic Photovoltaics on the World Community Grid. *The journal of physical chemistry letters* **2011**, *2*, 2241-2251.
37. Li, S.; Chung, Y. G.; Simon, C. M.; Snurr, R. Q. High-Throughput Computational Screening of Multivariate Metal-Organic Frameworks (MTV-MOFs) for CO₂ Capture. *The journal of physical chemistry letters* **2017**, *8*, 6135-6141.
38. Cheng, L.; Assary, R. S.; Qu, X.; Jain, A.; Ong, S. P.; Rajput, N. N.; Persson, K.; Curtiss, L. A. Accelerating Electrolyte Discovery for Energy Storage with High-Throughput Screening. *The journal of physical chemistry letters* **2015**, *6*, 283-291.
39. See Supplemental Material for computational method, magnetic configurations, bandstructure of some magnetic monolayers with high T_C, quantum anomalous Hall state in VCl₃, and tables of monolayer magnetic candidates.
40. Kurz, P.; Bihlmayer, G.; Blügel, S. Magnetism and electronic structure of hcp Gd and the Gd(0001) surface. *Journal of Physics: Condensed Matter* **2002**, *14*, 6353.
41. Hynninen, T.; Raebiger, H.; von Boehm, J.; Ayuela, A. High Curie temperatures in (Ga,Mn)N from Mn clustering. *Applied Physics Letters* **2006**, *88*, 122501.
42. Fuh, H. R.; Chang, C. R.; Wang, Y. K.; Evans, R. F.; Chantrell, R. W.; Jeng, H. T. Newtype single-layer magnetic semiconductor in transition-metal dichalcogenides VX₂ (X = S, Se and Te). *Sci. Rep.* **2016**, *6*, 32625.
43. Turek, I.; Kudrnovský, J.; Bihlmayer, G.; Blügel, S. Ab initio theory of exchange interactions and the Curie temperature of bulk Gd. *Journal of Physics: Condensed Matter* **2003**, *15*, 2771.
44. Liu, J.; Sun, Q.; Kawazoe, Y.; Jena, P. Exfoliating biocompatible ferromagnetic Cr-trihalide monolayers. *Phys Chem Chem Phys* **2016**, *18*, 8777-84.
45. Zhuang, H. L.; Xie, Y.; Kent, P. R. C.; Ganesh, P. Computational discovery of ferromagnetic semiconducting single-layer CrSnTe₃. *Phys. Rev. B* **2015**, *92*, 035407.
46. Ono, A.; Ishihara, S. Double-Exchange Interaction in Optically Induced Nonequilibrium State: A Conversion from Ferromagnetic to Antiferromagnetic Structure. *Phys. Rev. Lett.* **2017**, *119*, 207202.
47. Thielemann-Kühn, N.; Schick, D.; Pontius, N.; Trabant, C.; Mitzner, R.; Holldack, K.; Zabel, H.; Föhlisch, A.; Schübler-Langeheine, C. Ultrafast and Energy-Efficient Quenching of Spin Order: Antiferromagnetism Beats Ferromagnetism. *Phys. Rev. Lett.* **2017**, *119*, 197202.
48. Xiao, D.; Chang, M.-C.; Niu, Q. Berry phase effects on electronic properties. *Reviews of Modern Physics* **2010**, *82*, 1959-2007.
49. Xiao, D.; Yao, W.; Niu, Q. Valley-contrasting physics in graphene: magnetic moment and topological transport. *Phys. Rev. Lett.* **2007**, *99*, 236809.
50. Crisostomo, C. P.; Huang, Z.-Q.; Hsu, C.-H.; Chuang, F.-C.; Lin, H.; Bansil, A. Chemically induced large-gap quantum anomalous Hall insulator states in III-Bi honeycombs. *npj Computational Materials* **2017**, *3*, 39.
51. Schliemann, J.; MacDonald, A. H. Noncollinear ferromagnetism in (III,Mn)V semiconductors. *Phys. Rev. Lett.* **2002**, *88*, 137201.